J. Fluid Mech. (2008), *vol.* 605, *pp.* 389–400.
doi:10.1017/S0022112008001560 Printed in the United Kingdom

On the inviscid stability of bi-layer axisymmetric coatings

P. A. BLYTHE[1] AND P. G. SIMPKINS[2]

[1]Mechanical Engineering & Mechanics, Lehigh University, Bethlehem, PA 18015, USA
[2]College of Engineering, Syracuse University, Syracuse, NY 13244, USA

(Received 10 May 2007 and in revised form 17 March 2008)

This paper is concerned with the stability of fibre coatings at large Reynolds numbers. Both single- and double-layer coatings are considered; no restriction is placed on the coating thicknesses. Calculations for the maximum growth rate, together with the corresponding length scale of the instability, are presented. Rescaling with respect to the maximum growth rate generates universal dispersion relations over the unstable wavenumber range. For double-layer composite coatings, modifications are required when the density ratio becomes large.

1. Introduction

Liquid coatings are often applied to wires and fibres for insulation, protection and identification. During production, these coatings are susceptible to Rayleigh instabilities that can result in undesirable beading or diameter variations. In practice, the amplitudes of these disturbances are limited by solidifying the coating, either thermally or photo-chemically, prior to significant growth of the instability. Two-layer coatings are of particular relevance to optical fibres for which soft inner coatings and hard outer coatings are used. The inner coating minimizes micro-bending losses in the silica which affect the transmission quality of the signal; the outer coating protects the fibre integrity. Current indications are that future coating technologies will occur at higher Reynolds numbers so that viscous effects may play a smaller role. Many of the manufacturing techniques are designed to produce coatings whose thickness is comparable with the fiber radius. This paper is concerned with bi-layer coating instabilities in the inviscid limit when the Reynolds number is large. No restrictions on coating thicknesses are made.

Many of the earlier studies of coating flows have used the lubrication limit (see e.g. Landau & Levich 1942). A review of steady two-dimensional flows has been given by Weinstein & Ruschak (2004). Corresponding steady axially symmetric flows were considered by Bretherton (1961), and stability questions were examined, e.g. by Goren (1962) and Hammond (1983). Extensions to steady flows in which both axial and azimuthal curvature terms are important were made by Blythe & Simpkins (1995, 2004) and by Darhuber *et al.* (2000). Non-axially symmetric effects were discussed by Xu & Davis (1985) and by Russo & Steen (1989), and a general three-dimensional analysis has been developed by Ida & Miksis (1998*a*,*b*). Multi-layer films on inclined planes have been discussed, for example, by Wang, Seaborg & Lin (1978). Specific results for the stability of a three-layer film flow were obtained by Weinstein & Chen (1999). Recent work on polymeric bi-layer films has been presented by Jiang *et al.* (2006).

As noted above, increases in coating speeds, and the employment of metallic or similar coating materials, suggest the need for analyses with $Re \gg 1$ as opposed to lubrication theory. An outline of the single-layer inviscid theory can be found in Middleman (1995). In the present paper, it is demonstrated that the single-layer results for different coating thicknesses can be collapsed onto what is effectively a universal curve by employing a growth rate scaled with respect to its maximum value. Apparently, this result has not been previously recognized; it is a consequence of the small variation of the maximum growth wavenumber with thickness.

Much of the analysis in this paper addresses composite double-layer inviscid coating flows. No restrictions are placed on the relative thickness of the layers or on the density ratio of the coating fluids. Surface tension is included at the coating–air interface, but neglected elsewhere (see Weinstein & Chen 2004). Some industrial data indicate that this is a satisfactory assumption for certain immiscible materials that are soluble only in ketones. Under these conditions, the single-layer scaling argument can be extended to composite coatings. By normalizing the growth rate with respect to its maximum value, a remarkable collapse of the data is again obtained provided that the density ratio (outer/inner) is not large. The scaling law can be deduced from either physical reasoning or analytical arguments.

Appropriate non-dimensional forms of the linearized stability equations and their solution are presented in § 2, and the dispersion relation is derived. Numerical results for the growth rate of single-layer coatings are examined in § 3, where a determination of the maximum growth rate, including the corresponding instability length scale, is made. Simplified results for thin and thick coatings are also briefly described. Double-layer coatings are considered in § 4, where thickness and density ratio effects are discussed. Limiting cases for large density ratios and thin coatings require a special analysis. Asymptotic results for the growth rate in these limits are derived in the Appendix and a comparison with numerical calculations is given.

2. Formulation and the dispersion relations

After taking into account the relevant boundary conditions, the stability of an inviscid incompressible two-layer coating on a cylinder can be analysed in the manner described by Rayleigh (see Drazin & Reid 1982). Using cylindrical polar coordinates in a reference frame moving with the fiber, the base state is given by the steady constant thickness solution

$$w_j = u_j = 0, \quad \Delta P_i = \Delta P_o = 1, \quad r_o = 1 \ (r_i = \text{ const. } < 1), \tag{2.1}$$

where $j = i$ for the inner coating and $j = o$ for the outer coating. In (2.1), which also represents a solution of the viscous equations, (u, w) are the dimensionless velocity components in the radial and axial (r, z) directions. The velocities are made dimensionless with respect to the capillary speed $W_c = \sqrt{\sigma'/\rho'_o H'_\infty}$, the lengths with respect to the final combined coating radius H'_∞, the pressure difference ΔP_j with respect to σ'/H'_∞, and the time t using H'_∞/W_c. Here, σ' is the surface tension, and $\Delta P_j = P_j - P_a$ where P_a denotes the external (fixed) atmospheric pressure. At the fibre surface

$$u_i = 0 \quad \text{on} \quad r = r_f (\equiv r'_f/H'_\infty). \tag{2.2}$$

On the interface, surface tension is neglected so that

$$P_i = P_o \quad \text{on} \quad r = r_i. \tag{2.3}$$

At the interface and the free surface, the kinematic conditions are

$$u_j = \frac{\partial r_j}{\partial t} + w_j \frac{\partial r_j}{\partial z}. \tag{2.4}$$

Surface tension is included at the free surface, where the normal stress balance becomes

$$\Delta P_o = P_o - P_a = \frac{1}{r_o(1+(\partial r_o/\partial z)^2)^{1/2}} - \frac{\partial^2 r_o/\partial z^2}{(1+(\partial r_o/\partial z)^2)^{3/2}}. \tag{2.5}$$

Linearized perturbations about this constant state, with

$$\Delta P_j = 1 + p_j, \quad \Delta r_j = h_j, \tag{2.6}$$

are taken to be of the axially symmetric form

$$\left[u_j, w_j, p_j, h_j\right] = \left[\bar{u}_j(r), \bar{w}_j(r), \bar{p}_j(r), \bar{h}_j\right] \exp(\alpha t + \mathrm{i}kz). \tag{2.7}$$

(It can be shown that weak asymmetric disturbances are neutrally stable.) The amplitude of the pressure perturbation $\bar{p}$ satisfies Bessel's equation

$$r^2 \frac{\mathrm{d}^2 \bar{p}}{\mathrm{d}r^2} + r \frac{\mathrm{d}\bar{p}}{\mathrm{d}r} - k^2 r^2 \bar{p} = 0, \tag{2.8}$$

for which the solution, in each layer, is

$$\bar{p} = A_j I_0(\zeta) + B_j K_0(\zeta) \tag{2.9}$$

with

$$\bar{w} = -\frac{\mathrm{i}k}{\alpha}\bar{\rho}_j\{A_j I_0(\zeta) + B_j K_0(\zeta)\}, \quad \bar{u} = -\frac{k}{\alpha}\bar{\rho}_j\{A_j I_1(\zeta) - B_j K_1(\zeta)\}, \tag{2.10}$$

where $I_n(\zeta)$ and $K_n(\zeta)$ are modified Bessel functions, $\zeta = kr$ and $\bar{\rho}_j = \rho_o'/\rho_j'$. The boundary and interface conditions (2.2)–(2.5) require that

$$\bar{u}_i(r_f) = 0, \quad \bar{u}_i(r_i) = \alpha\bar{h}_i = \bar{u}_o(r_i), \quad \bar{p}_i(r_i) = \bar{p}_o(r_i), \tag{2.11}$$

$$\bar{u}_o(1) = \alpha\bar{h}_o, \quad \bar{p}_o(1) = -(1-k^2)\bar{h}_o. \tag{2.12}$$

Manipulations based on these conditions lead to

$$\frac{\alpha^2}{k(1-k^2)} = N = \frac{D_1(\zeta_f, k) + (1-\bar{\rho})\zeta_i D_1(\zeta_i, \zeta_f) S(\zeta_i, k)}{S(k, \zeta_f) - (1-\bar{\rho})\zeta_i D_1(\zeta_i, \zeta_f) D_0(k, \zeta_i)}, \tag{2.13}$$

where $\bar{\rho} = \rho_o/\rho_i$, $\zeta_i = kr_i$ and $\zeta_f = kr_f$. In (2.13)

$$S(x, y) = K_0(x)I_1(y) + K_1(y)I_0(x), \tag{2.14}$$

$$D_n(x, y) = K_n(x)I_n(y) - K_n(y)I_n(x). \tag{2.15}$$

Equation (2.13), and the ancillary expressions (2.14) and (2.15), represent the dispersion relation for the stability of the bi-layer coating flow.

3. Single-layer behaviour

When the density ratio $\bar{\rho} = 1$, (2.13) reduces to

$$N \equiv \frac{\alpha^2}{k(1-k^2)} = \frac{D_1(\zeta_f, k)}{S(k, \zeta_f)} = \frac{K_1(\zeta_f)I_1(k) - K_1(k)I_1(\zeta_f)}{K_0(k)I_1(\zeta_f) + K_1(\zeta_f)I_0(k)}, \tag{3.1}$$

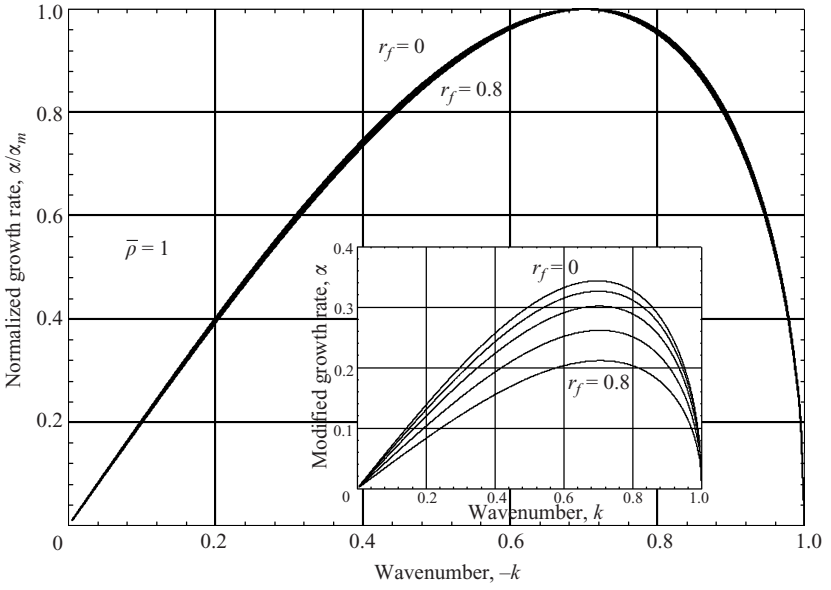

FIGURE 1. Growth rates normalized by α_m. The inset shows the modified growth rate dependence on r_f (lines are, from the top, $r_f = 0$, 0.33, 0.5, 0.67, 0.8).

which is the single-layer result (see e.g. Middleman 1995). Standard results for this case are briefly reviewed below.

For thin coatings ($1 - r_f \ll 1$) it can be shown that

$$\alpha^2 = k^2(1 - k^2)(1 - r_f), \tag{3.2}$$

and only wavenumbers with $|k| < 1$ are unstable. The maximum growth rate arises when $k^2 = k_m^2 = 1/2$. Similarly, for thick coatings ($r_f \to 0$), (3.1) gives

$$\alpha^2 = k(1 - k^2)\frac{I_1(k)}{I_0(k)}. \tag{3.3}$$

This result is equivalent to that for an inviscid liquid jet (see Middleman 1995). Again, only wavenumbers with $|k| < 1$ are unstable, but now the maximum growth rate occurs at $k_m \approx 0.6970$, i.e. close to the zero thickness limit $1/\sqrt{2} \approx 0.7071$.

For general values of r_f, it follows from (3.1) that $N > 0$ for $|k| < 1$, and unstable disturbances arise only when $|k| < 1$. The current linear theory indicates that disturbances with $|k| > 1$ are neutrally stable. Growth rates for various fibre radii r_f are shown in figure 1 (inset). As observed above, there is little variation in the wavenumbers k_m that correspond to the maximum growth rate. In fact, replotting the data after normalizing with respect to the maximum α for a specific r_f, i.e. $\alpha = \alpha_m(r_f)$, gives the result shown in figure 1.

As can be seen, this simple scaling essentially leads to a universal curve, and was noted by Blythe & Simpkins (2002). The small variation in the value of $k = k_m$, corresponding to $\alpha_m(r_f)$, is shown in figure 2, where the change in k_m is less than 1.5% over the entire range of r_f. Results for $\alpha_m(r_f)$ are discussed below in §4. Collapsing the dispersion curves in this way has not been previously observed.

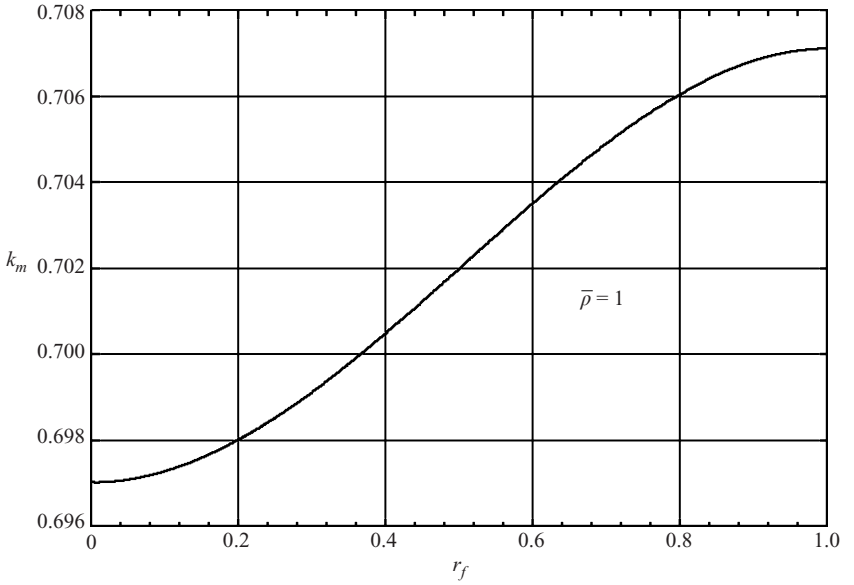

FIGURE 2. Wavenumbers at α_m for various values of r_f.

4. Bi-layer results

4.1. *Variable thickness effects*

Double-layer stability results depend on the thickness ratio

$$\tau = \frac{r_o - r_i}{r_i - r_f}, \tag{4.1}$$

where r_f, r_i and r_o ($\equiv 1$) are, respectively, the dimensionless fiber, interface and outer radii. The dispersion relation (2.13) is displayed in figure 3 (inset) for different thickness ratios when $r_f = 0.5$ and $\bar{\rho} = 0.5$.

Single-layer results given in § 3 suggest that it is appropriate to normalize the growth rate by its maximum value $\alpha_m(r_f, \tau)$. This also effectively collapses the data onto the single curve shown in figure 3. Similar results arise for various fiber radii r_f at a fixed thickness ratio τ.

Remarkably, both the single-layer results and the bi-layer results collapse in the manner shown in figure 3. Results for a variety of different values of $r_f, \tau,$ and $\bar{\rho}$ are displayed in this figure. For all data displayed in figure 3, $\bar{\rho} < 10$. Each curve is well represented by the thin single-layer limit (3.2), i.e.

$$\frac{\alpha}{\alpha_m} = 2k\sqrt{1 - k^2}. \tag{4.2}$$

The variation in the maximum growth rate α_m with r_f is shown in figure 4 for various thickness ratios τ. For $r_f = 0$, the results correspond to a composite jet. As $\tau \to \infty$ (vanishingly thin inner layer, $r_i \to r_f$), the single-layer solution (3.1) is recovered, and as $\tau \to 0$ (thin outer layer, $r_i \to r_o$), the single-layer result (3.1), now pre-multiplied by a factor $\bar{\rho}$, is also obtained. Values obtained from these limiting cases, including (3.3), are in complete agreement with numerical calculations using the bi-layer dispersion relation (2.13).

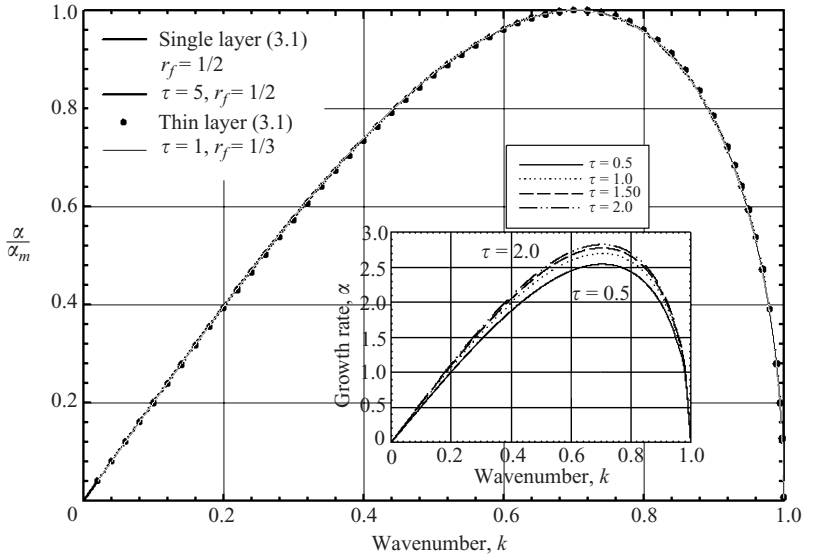

FIGURE 3. Total collapse of single-layer and bi-layer results. The inset shows the growth-rate dependence on the thickness ratio where $r_f = 0.5; \bar{\rho} = 0.5$.

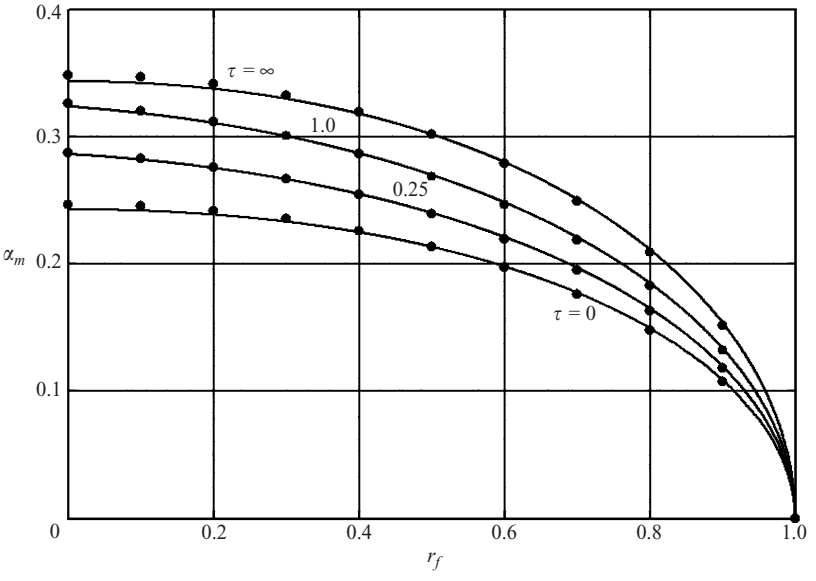

FIGURE 4. Maximum growth rate for various thickness ratios; $\bar{\rho} = 0.5$; •, equation (4.5).

All the above results for α/α_m are consistent with the universal behaviour shown in figure 3, which suggests that

$$\alpha_m \propto \text{ gradient at } k = 0. \tag{4.3}$$

From the dispersion relation (2.13), and the limiting results for S and D_n as $k \to 0$, it can be established that

$$\left.\frac{\mathrm{d}\alpha}{\mathrm{d}k}\right|_{k=0} = \sqrt{\frac{1 - r_f^2 - (1-\bar{\rho})(r_i^2 - r_f^2)}{2}}. \tag{4.4}$$

The scaling postulate (4.3) then implies

$$\alpha_m = m\sqrt{\frac{1 - r_f^2 - (1-\bar{\rho})\left(r_i^2 - r_f^2\right)}{2}}. \tag{4.5}$$

Based on the single-layer results, the constant m is bounded by the thin film and jet limits. Specifically,

$$0.48555 \leqslant m \leqslant 0.5. \tag{4.6}$$

Comparisons between (4.5) and the numerical calculations are shown in figure 4, where the mean value of m based on (4.6) is used. Excellent agreement is found. Note that the results for $\tau = \infty$ correspond to the single-layer solution outlined earlier in § 3.

The scaling law (4.5) can also be obtained from physical arguments by viewing the coating layers as fixed control volumes of length L'. Momentum balances in the z-direction give, for each annulus,

$$\rho_j' L' A_{cj}' \frac{\Delta w_j'}{\Delta t'} = \Delta P' A_{cj}', \tag{4.7}$$

where primed variables are dimensional. In (4.7), Δ denotes the overall change in the axial direction, and A_{cj}' is the annulus cross-sectional area. If the axial pressure difference is the same for both layers, then

$$\rho_i' \Delta w_i' = \rho_o' \Delta w_o', \quad \Delta t' = \rho_o' \frac{L' \Delta w_o'}{\Delta p'}. \tag{4.8}$$

The free-surface displacement, $h' = r' - H_\infty'$, gives rise through surface tension to changes in the normal stress with $\Delta p' = -\sigma' c \Delta h' / H_\infty'^2$, where c/H_∞' corresponds to the mean curvature. In addition, the kinematic condition on the outer surface requires that $\Delta h' = u_o' \Delta t'$ where u_o' is the radial velocity component. Consequently, the growth rate

$$\alpha' = \frac{1}{\Delta t'} = \sqrt{\frac{c\sigma'(-u_o')}{\rho_o' r_o'^2 L' \Delta w_o'}}. \tag{4.9}$$

Conservation of volume flow for the two layers requires that

$$\Delta w_i' A_{ci}' + \Delta w_o' A_{co}' + 2\pi H_\infty' L' u_o' = 0. \tag{4.10}$$

Using the above relations, and introducing the dimensionless variables of § 2, gives

$$\alpha^2 = \tfrac{1}{2}\left[1 - r_f^2 - (1-\bar{\rho})\left(r_i^2 - r_f^2\right)\right] k^2 (1 - k^2), \tag{4.11}$$

where the choices $L' = H_\infty'/k$ and $c = 1 - k^2$ have been made, and the expression for c incorporates the second curvature term in the normal stress condition. Equation (4.11) is consistent with (4.5) when $m = 0.5$.

4.2. *Influence of the density ratio*

Although the universal curves are presented for $\bar{\rho} = 0.5$, this normalization holds for density ratios less than about 10. As the density ratio increases, however, the wavenumber k_m for maximum growth depends strongly on $\bar{\rho}$. Figure 5 displays computations for the dependence of the growth rate on the density ratio. Here, the results are given for a thickness ratio $\tau = 1$ and a dimensionless fiber radius of 0.5, but similar trends occur for other values of τ and r_f.

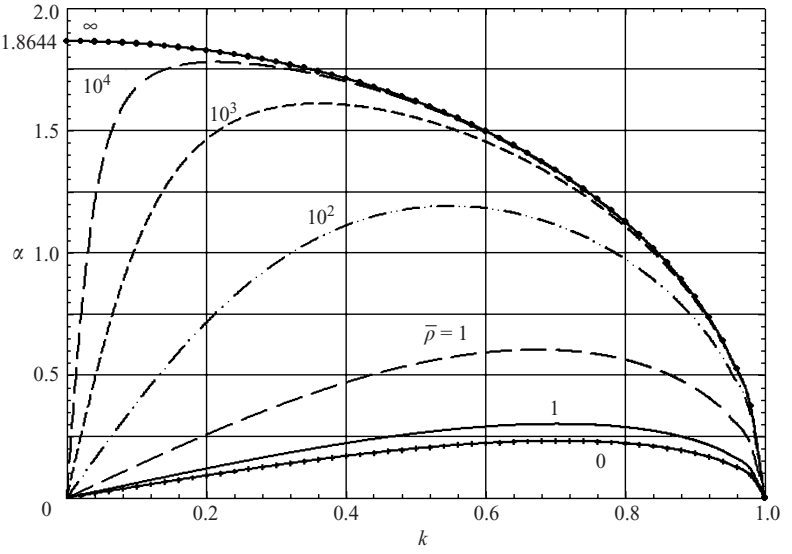

FIGURE 5. The influence of density ratio for $r_f = 0.5$ and $\tau = 1$. +, equation (4.12); •, equation (4.13).

As $\bar{\rho} \to 0$, it can be deduced from (2.13) that

$$\frac{\alpha^2}{k(1-k^2)} \to \frac{D_1(\zeta_f, k) + \zeta_i D_1(\zeta_i, \zeta_f) S(\zeta_i, k)}{S(k, \zeta_f) - \zeta_i D_1(\zeta_i, \zeta_f) D_0(k, \zeta_i)}. \tag{4.12}$$

The limiting profile defined by (4.12) is shown in figure 5.

For increasing $\bar{\rho}$, the location of the maximum growth rate approaches $k = 0$. Away from $k = 0$, the limiting profile as $\bar{\rho} \to \infty$ is given by

$$\alpha^2 = -k(1-k^2)\frac{S(\zeta_i, k)}{D_0(k, \zeta_i)}. \tag{4.13}$$

This limiting case is also displayed in figure 5, together with results for intermediate values of $\bar{\rho}$. Curves of $k_m(r_f; \bar{\rho})$ are given in figure 6, which shows that there is a rapid variation in k_m at large $\bar{\rho}$ as $r_f \to 1$. Consequently, the universal scaling presented in figure 3 is not valid in this limit.

The dependence of the maximum growth rate on r_f is shown in figure 7 for various density ratios. It is apparent from figures 5 to 7 that a different approach is required for $\bar{\rho} \gg 1$. Details of the behaviour when the density ratio is large are given in the Appendix.

5. Concluding remarks

For single-layer coatings, it was demonstrated in § 3 that normalizing the growth rates by their maximum values leads to a universal curve. In § 4, this approach was extended to bi-layer films. The data for various thickness ratios, and for various fiber radii, also collapse onto a universal curve when the density ratio $\bar{\rho} < 10$. Scaling arguments and physical considerations both lead to the same prediction for the maximum growth rate that is in excellent agreement with the full dispersion relation.

At larger values of $\bar{\rho}$, the instability growth rate is more sensitive to the magnitude of the density ratio. Numerical results indicate the presence of severe spikes in the

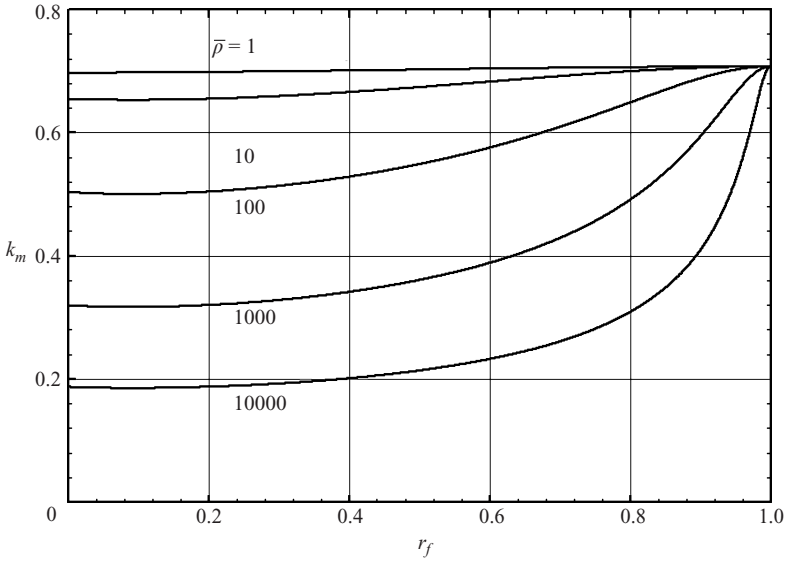

FIGURE 6. Maximum growth wavenumber: $\tau = 1$.

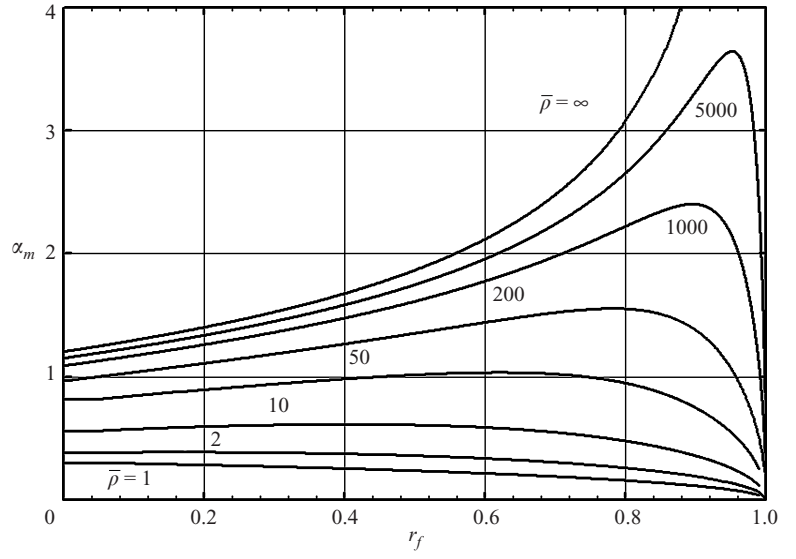

FIGURE 7. Maximum modified growth rate for various density ratio, $\tau = 1$.

growth rate when the overall layer thickness is small. Asymptotic results developed for large density ratios and thin films are in excellent agreement with the numerical calculations (see Appendix).

Part of this work was carried out while P. G. S. was at Bell Laboratories, Murray Hill, NJ 07974, USA. The authors are grateful to the referees for helpful comments.

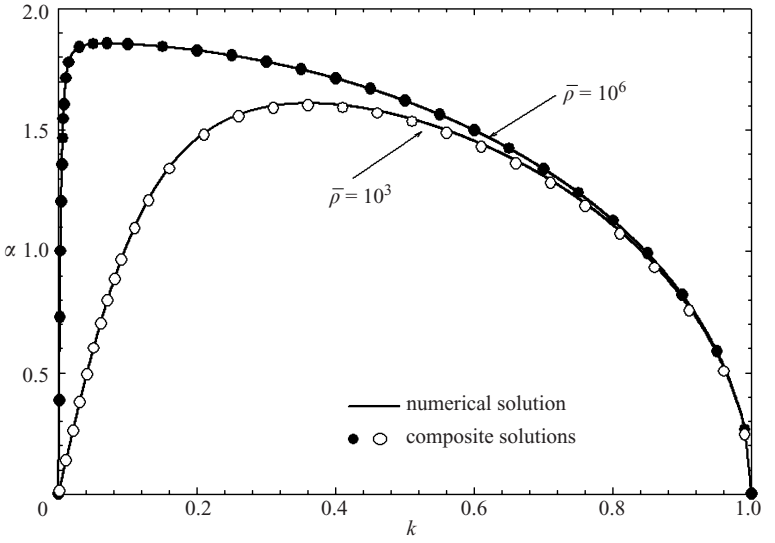

FIGURE 8. Overall structure: composite solution $\bar{\rho} \gg 1$. $\tau = 1$; $r_f = 0.5$.

Appendix. Large density ratio asymptotics

If $\bar{\rho} \gg 1$, the limiting behaviour associated with the large gradients that arise near $k = 0$ requires an appropriate boundary-layer description (figure 8). Expanding (2.13) as $k \to 0$, at fixed $\bar{\rho}$, τ and r_f, suggests that non-uniformities occur when $\bar{\rho} = O(k^{-2})$. Within this boundary layer, an appropriate scaled wavenumber ($\bar{\rho} \to \infty$) is $\kappa = \sqrt{\bar{\rho}}\, k$. Using κ and (2.13), it is found that near $k = 0$

$$\alpha^2 = \frac{\left(r_i^2 - r_f^2\right)\kappa^2}{2 + \left(r_i^2 - r_f^2\right)\ln(1/r_i)\kappa^2}, \tag{A1}$$

which matches with (4.13) as $\kappa \to \infty$. From (4.13) and (A1) a suitable leading-order composite solution, valid for $0 \leqslant k \leqslant 1$, can also be constructed. Specifically,

$$\alpha_{comp} = \sqrt{\frac{\left(r_i^2 - r_f^2\right)\kappa^2}{2 + \left(r_i^2 - r_f^2\right)\ln(1/r_i)\kappa^2}} + \sqrt{-k(1-k^2)\frac{S(\zeta_i, k)}{D_0(k, \zeta_i)}} - \sqrt{\frac{1}{\ln(1/r_i)}}. \tag{A2}$$

Comparisons with the exact solution (2.13) are shown in figure 8.

From figure 7, it can be seen that when $\bar{\rho} \gg 1$ further resolution is required as $r_f \to 1$. A suitable distinguished limit corresponds to thin films with $\bar{\rho}(1 - r_f)^2 = O(1)$. For thickness ratios $\tau = O(1)$, substitution into (2.13), neglecting relative error terms $O((1 - r_f)^2)$, leads to

$$\alpha^2 = \frac{\left[1 - \frac{1}{2}s(1 - r_f)\right]}{s(1 - r_f)} \frac{\bar{\lambda}k^2(1 - k^2)}{1 + \bar{\lambda}k^2} \tag{A3}$$

where

$$\lambda = s(1 - s)\bar{\rho}(1 - r_f)^2, \quad s = \tau/(1 + \tau), \quad \bar{\lambda} = \left(1 - \tfrac{1}{2}(1 - r_f)\right)\lambda. \tag{A4}$$

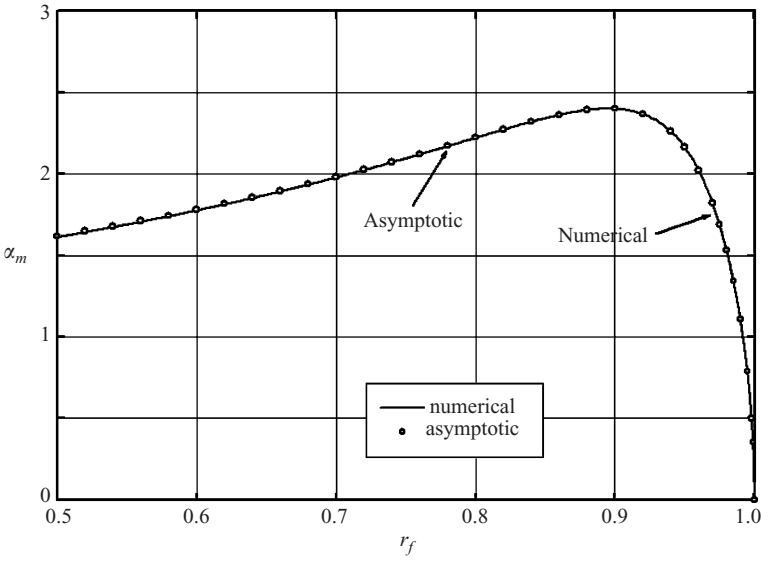

FIGURE 9. Boundary-layer structure for $\bar{\rho} = 10^3$. $\tau = 1$.

From (A3) it is readily established that the wavenumber corresponding to the maximum growth rate is defined by

$$k_m^2 = \frac{\sqrt{1+\bar{\lambda}}-1}{\bar{\lambda}} \quad \text{with} \quad \alpha_m^2 = \frac{\left[1-\frac{1}{2}s(1-r_f)\right]}{s(1-r_f)}\,\frac{(2+\bar{\lambda}-2\sqrt{1+\bar{\lambda}})}{\bar{\lambda}} \tag{A5}$$

A typical plot of $\alpha_m(r_f)$, with $\bar{\rho} = 10^3$ and $\tau = 1$, is shown in figure 9. Excellent agreement with numerical calculations based on the full dispersion relation is found even at $r_f = 0.5$. When $\bar{\rho} \gg 1$, a feature of these curves is the peak in the maximum growth rate for $r_f \to 1$ (see figure 7). Based on (A5), the leading approximation for the location of the peak is $\bar{\lambda} = \bar{\lambda}_0 = 3$. It follows that the locus of the peak, neglecting terms $O(\bar{\rho}^{-3/4})$, is

$$\alpha_{m_{\max}} = 3^{-3/4}\left(\frac{1-s}{s}\right)^{1/4}\left(1-\frac{\sqrt{3}}{2}\varepsilon\right)\bar{\rho}^{1/4} \quad \text{where } \varepsilon = \frac{\left(\frac{1}{4}+\frac{1}{2}s\right)}{\sqrt{s(1-s)}}\bar{\rho}^{-1/2} \ll 1. \tag{A6}$$

Values of $r_f = r_{fm}(\bar{\rho})$ that correspond to the peak in the maximum growth rate are defined by

$$1 - r_{f_m} = \sqrt{\frac{3}{s(1-s)}}\bar{\rho}^{-1/2}\left\{1-\left(\frac{(1+8s)\sqrt{3}}{12\sqrt{s(1-s)}}\right)\bar{\rho}^{-1/2}\right\}. \tag{A7}$$

Predictions from (A6) and (A7) also agree closely with numerical calculations.

REFERENCES

BLYTHE, P. A. & SIMPKINS, P. G. 1995 Fiber coating thickness predictions at low capillary numbers. *Bull. Am. Phys. Soc.* **40**, 2016.

BLYTHE, P. A. & SIMPKINS, P. G. 2002 Fiber coating instabilities: the inviscid limit. *OFS Fitel Tech. Memo.*

Blythe, P. A. & Simpkins, P. G. 2004 Fibre coating: non-unique solutions at small capillary numbers. *J. Fluid Mech.* **515**, 353.

Bretherton, F. P. 1961 The motion of long bubbles in tubes. *J. Fluid Mech.* **10**, 166.

Darhuber, A. A., Trojan, S. M., Davis, J. M. & Miller, S. M. 2000 Selective dip-coating of chemically micro-patterned surfaces. *J. Appl. Phys.* **88**, 5119.

Drazin, P. G. & Reid, W. H. 1982 Hydrodynamic Stability, Chap. 1, § 5. Cambridge University Press.

Goren, S. L. 1962 The instability of an annular thread of fluid. *J. Fluid Mech.* **12**, 309.

Hammond, P. S. 1983 Nonlinear adjustment of a thin annular film of viscous fluid surrounding a thread of another within a circular cylindrical pipe. *J. Fluid Mech.* 137, 363.

Ida, M. P. & Miksis, M. J. 1998*a* The dynamics of thin films; I General theory. *SIAM J. Appl. Maths.* **58**, 456.

Ida, M. P. & Miksis, M. J. 1998*b* The dynamics of thin films; II Applications. *SIAM J. Appl. Maths.* **58**, 474.

Jiang, Z., Kim, H., Mochrie, S. G. J., Lurio, L. B. & Sinha, S. K. 2006 Surface and interfacial dynamics of polymeric bilayer films. *Phys. Rev.* E **74**, 11603.

Landau, L. & Levich, B. 1942 Dragging of a liquid by a moving plate. *Acta Physiochim. USSR* **17**, 42.

Middleman, S. 1995 *Modeling Axisymmetric Flows: Dynamics of Films, Jets, and Drops*, chap. 4, pp. 105 *et seq.* Academic.

Russo, M. J. & Steen, P. H. 1989 Shear stabilization of the capillary breakup of a cylindrical interface. *Phys. Fluids* A **1**, 1926.

Wang, C. K., Seaborg, J. J. & Lin, S. P. 1978 Instability of multi-layered liquid films. *Phys. Fluids* **21**, 1669.

Weinstein, S. J. & Chen, K. P. 1999 Large growth rate instabilities in three-layer flow down an incline in the limit of zero Reynolds number. *Phys. Fluids* **11**, 3270.

Weinstein, S. J. & Ruschak, K. J. 2004 Coating flows. *Ann. Rev. Fluid Mech.* **36**, 29.

Xu, Z. Z. & Davis, S.H. 1985 Instability of capillary jets with thermocapillarity. *J. Fluid Mech.* **161**, 1.